Cement & Concrete Composites 55 (2015) 383–394

Contents lists available at ScienceDirect

Cement & Concrete Composites

journal homepage: www.elsevier.com/locate/cemconcomp

Development of an eco-friendly Ultra-High Performance Concrete (UHPC) with efficient cement and mineral admixtures uses

R. Yu [a,*], P. Spiesz [a,b], H.J.H. Brouwers [a]

[a] Department of the Built Environment, Eindhoven University of Technology, P.O. Box 513, 5600 MB Eindhoven, The Netherlands
[b] HeidelbergCement Benelux, The Netherlands

ARTICLE INFO

Article history:
Received 16 June 2014
Received in revised form 19 September 2014
Accepted 29 September 2014
Available online 18 October 2014

Keywords:
Eco-friendly
Ultra-High Performance Concrete (UHPC)
Modified Andreasen & Andersen particle packing model
Efficient uses
Mineral admixtures
Embedded CO_2

ABSTRACT

This paper addresses the development of an eco-friendly Ultra-High Performance Concrete (UHPC) with efficient cement and mineral admixtures uses are investigated. The modified Andreasen & Andersen particle packing model is utilized to achieve a densely compacted cementitious matrix. Fly ash (FA), ground granulated blast-furnace slag (GGBS) and limestone powder (LP) are used to replace cement, and their effects on the properties of the designed UHPC are analyzed. The results show that the influence of FA, GGBS or LP on the early hydration kinetics of the UHPC is very similar during the initial five days, while the hydration rate of the blends with GGBS is mostly accelerated afterwards. Moreover, the mechanical properties of the mixture with GGBS are superior, compared to that with FA or LP at both 28 and 91 days. Due to the very low water amount and relatively large superplasticizer dosage in UHPC, the pozzolanic reaction of FA is significantly retarded. Additionally, the calculations of the embedded CO_2 emission demonstrate that the cement and mineral admixtures are efficiently used in the developed UHPC, which reduce its environmental impact compared to other UHPCs found in the literature.

1. Introduction

Since 1980s, High Strength Concrete (HSC) has attracted a lot of attention, which later triggered the development of Reactive Powder Concrete (RPC) [1–3]. In the components of RPC, coarse aggregates are normally eliminated with active powders (e.g. cement, ground granulated blast-furnace, silica fume) as the main ingredients. Due to the relatively dense and homogenous microstructure of RPC, its maximum compressive strength can even exceed 200 MPa [4,5]. However, with the quickly developing construction industry, concrete expect the compressive strength is also required to have high flexural strength, workability and durability, which resulted the development of Ultra-High Performance Concrete (UHPC) and Ultra-High Performance Fibre Reinforced Concrete (UHPFRC) [6–8]. Nevertheless, as the sustainable development is currently a pressing global issue and various industries have strived to achieve energy savings, the high material cost, high energy consumption and CO_2 emission for UHPC are the typical disadvantages that restrict its wider application [9–11]. Hence, how to efficiently produce UHPC, based on materials point of view, still needs further investigation.

By far, the measures pursued to reduce the economic and environmental disadvantages of UHPC are limited in most cases to the application of industrial by-products or waste materials without sacrificing the UHPC performance [7,8,12–15]. Nevertheless, in most cases in the literature, for the mix design of UHPC, the amounts of mineral admixtures (e.g. fly ash (FA), ground granulated blast-furnace (GGBS), limestone powder (LP) and silica fume (SF)) are given directly, without any detailed explanations or theoretical support. Moreover, due to the complex cementitious system of UHPC (extremely low water amount and relatively high SP content), the influence of different mineral admixtures on the hydration kinetics and properties of UHPC still needs further clarification [6–8,11–15]. As commonly known, GGBS has hydraulic properties although the rate of the reaction with water is low [16]. The reaction can be activated by several methods, but the hydration product is always C–S–H. In blended cements, GGBS is chemically activated by $Ca(OH)_2$ and gypsum [17,18]. In most cases, GGBS reacts very fast, which causes that the enhancement of mechanical properties of mortar or concrete with GGBS can be observed already during the early age [19–21]. On the contrary, the pozzolanic reaction of FA is relatively slow, and the addition of FA can retard the hydration of cement [22–24]. The retardation phenomenon is related to the presence and properties of FA. It is suggested that the FA surface acts somewhat like a calcium-sink, and calcium in solution is removed by the abundant aluminum

* Corresponding author. Tel.: +31 (0) 40 247 5469; fax: +31 (0) 40 243 8595.
E-mail address: r.yu@tue.nl (R. Yu).

http://dx.doi.org/10.1016/j.cemconcomp.2014.09.024
0958-9465/

Nomenclature

b	empirical constant, –
d_0	base diameter of the used cone, mm
d_1	diameter of the spread concrete mixtures, mm
d_2	diameter of the spread concrete mixtures (perpendicular to d_1), mm
D	particle size, μm
D_{max}	maximum particle size, μm
D_{min}	minimum particle size, μm
k	empirical constant, –
m_d	mass of oven dried sample, g
m_s	mass of surface dried and water-saturated sample in air, g
m_w	hydrostatic mass of water-saturated sample in water, g
$m_{w\text{-}p}$	water demand of powder materials (from Puntke test), g
p	porosity of material, %
p_c	percolation porosity at failure threshold, %
P_{mix}	composed mix, –
P_{tar}	target curve, –
$P(D)$	fraction of the total solids being smaller than size D, –
q	distribution modulus, –
RSS	sum of the squares of the residuals, –
V_w	volumetric water demand of the powder material for saturation, cm^3
V_p	volume of the tested powder material, cm^3
φ	computed void fraction, %
$\varphi_{v,water}$	water-permeable porosity, %
σ	strength of the tested material, MPa
σ_0	strength of material at zero porosity, MPa
ρ_s	specific density, g/cm^3
$\xi_{Reschke}$	particle shape factor, –
ψ	void faction of the saturated powder material, –

associated with FA, as AFt phases preferentially forms on the surface of FA [22,23]. This depresses the Ca^{2+} concentration in solution during the first 6 h of hydration, and the formation of a Ca-rich surface layer on the clinker minerals is also postponed [22,23]. Therefore, the $Ca(OH)_2$ and C–S–H nucleation and crystallization are delayed and the cement hydration is simultaneously retarded [23]. Nevertheless, with a slow increase of the $Ca(OH)_2$ concentration in normal strength concrete (NSC), the pozzolanic reaction of FA can be further proceeded and the mechanical properties of NSC at 91 days can be further enhanced [25–27]. Additionally, the activity of LP in the cementitious system is still under debate. Many researchers treat LP as a filler and have experimentally demonstrated that the principal properties of cement are not negatively affected if small quantities of LP (5–6%) are added during the cement grinding [28–31]. On the other hand, some investigations [32–34] showed that, during the hydration process of cement with LP, tri-calcium aluminate (C_3A) can react with calcium carbonate to form both high- and low carbonate forms of calcium carboaluminate (CCA) in much the same manner as C_3A reacts with calcium sulfate to form high- and low-sulfate forms of calcium sulpoaluminate (CSA). Furthermore, the reaction of LP largely depends on its fineness, which can be demonstrated by the phenomenon that the LP with d_{50} of about 0.7 μm could effectively enhance the heat flow of cement during the hydration process [35]. Although a significant amount of investigations regarding the effect of mineral admixtures on the physical and chemical characteristics of mortar or concrete can be easily found, they all focus only on NSC, in which the water to binder ratio is relatively high and very limited SP dosage is utilized. However, the cementitious system of UHPC is very different from that of NSC, which cause that it is difficult to evaluate the influence of mineral admixtures on the cement hydration and properties development of UHPC, based on the knowledge obtained from NSC. Therefore, to efficiently develop UHPC, it is important to understand the effect of different mineral admixtures on the properties and hydration process of UHPC.

For the design of mortars and concretes, several mix design tools are in use. Based on the properties of multimodal, discretely sized particles, De Larrard and Sedran [36,37] postulated different approaches to design concrete: the Linear Packing Density Model (LPDM), Solid Suspension Model (SSM) and Compressive Packing Model (CPM). Furthermore, Fennis et al. [38] developed a concrete mix design method based on the concepts of De Larrard and Sedran [36,37]. However, all these design methods are based on the packing fraction of individual solid components (cement, sand, etc.) and their combinations, and therefore it is complicated to include very fine particles in these mix design tools, as it is difficult to determine the packing fraction of such fine materials or their combinations. Another possibility for mix design is offered by an integral particle size distribution approach of continuously graded mixes (modified Andreasen & Andersen particle packing model), in which very fine particles can be integrated with considerably lower effort, as detailed in [39]. Additionally, based on the previous experiences and investigations of the authors [40–42,73], by applying this modified Andreasen & Andersen particle packing model, it is possible to produce a dense and homogeneous skeleton of UHPC or UHPFRC with a relatively low binder amount (about 650 kg/m^3). Consequently, it can be shortly concluded that such an optimized design of concrete with appropriate amount of mineral admixtures can be a promising approach to produce Ultra-High Performance Concrete (UHPC) in an efficient way.

In general, based on these premises, the objective of this study is to develop UHPC and evaluate the influence of different mineral admixtures on the fresh and hardened behavior, hydration kinetics and thermal properties of the developed UHPC. Techniques such as isothermal calorimetry, thermal analysis and scanning electron microscopy are employed to investigate the hydration mechanism and microstructure development of concrete. Additionally, to evaluate the environmental impacts of the designed UHPC, its embedded CO_2 emission is calculated and compared with that of UHPCs found in the literature.

2. Materials and experimental methodology

2.1. Materials

The cement used in this study is Ordinary Portland Cement (OPC) CEM I 52.5 R, provided by ENCI (the Netherlands). A polycarboxylic ether based superplasticizer is used to adjust the workability of UHPC. The FA, GGBS and LP are used to replace cement. Two types of sand are used, one is a normal sand with the fraction 0–2 mm and the other one is a micro-sand with the fraction 0–1 mm (Graniet-Import Benelux, the Netherlands). One type of nano-silica slurry is selected as an high active pozzolanic material in this study. More detailed information and characteristics of the used materials are shown in Tables 1–4 and Figs. 1 and 2. It can be noticed that the particle size distribution of the used FA, GGBS and LP is comparable to that of cement. Therefore, when the cement is replaced by FA, GGBS or LP, the particle packing of the whole solid skeleton is only slightly affected.

Table 1
Materials types and densities.

Materials	Type	Specific density (kg/m^3)	Pozzolanic activity index (28 days)
Cement	CEM I 52.5 R	3150	–
FA	–	2293	83
GGBS	–	2893	96
LP	–	2710	–
Fine sand	Micro-sand	2720	–
Coarse sand	Sand 0–2	2640	–
Superplasticizer	Polycarboxylate ether	1050	–
Pozzolanic material	Nano-silica (nS)	2200	113

Table 2
Characterization of the used nano-silica.[a]

Type	Slurry
Stabilizing agent	Ammonia
Specific density (g/cm^3)	2.2
pH (at 20 °C)	9.0–10.0
Solid content (% w/w)	20
Viscosity (mPa s)	⩽100
BET (m^2/g)	22.7
PSD by LLS (μm)	0.05–0.3
Mean particle size (μm)	0.12

[a] Data obtained from the supplier.

Table 3
Characteristics of the powder materials.

Materials	Specific density, ρ_s (g/cm^3)	Water demand (Puntke test),[a] $m_{w\text{-}p}$ (g)	Computed void fraction, φ (%)	Particle shape factor, $\xi_{Reschke}$ (–)
CEM I 52.5 R	3.15	13.2	45.4	1.68
LP	2.72	10.8	37.0	1.26
FA	2.29	11.2	33.9	1.20
GGBS	2.89	13.2	43.3	1.58

[a] The Puntke test is executed following the reference shown in [48].

Table 4
Oxide composition of cement, FA, GGBS, LP and nS.

Substance	Cement (mass%)	FA (mass%)	GGBS (mass%)	LP (mass%)	nS (mass%)
CaO	64.60	4.46	38.89	89.56	0.08
SiO_2	20.08	55.32	34.18	4.36	98.68
Al_2O_3	4.98	22.45	13.63	1.00	0.37
Fe_2O_3	3.24	8.52	0.51	1.60	–
K_2O	0.53	2.26	0.43	0.34	0.35
Na_2O	0.27	1.65	0.33	0.21	0.32
SO_3	3.13	1.39	1.41	–	–
MgO	1.98	1.89	10.62	1.01	–
TiO_2	0.30	1.17	–	0.06	0.01
Mn_3O_4	0.10	0.11	–	1.605	–
P_2O_5	0.74	0.76	–	0.241	0.15
Cl^-	0.05	0.02	–	–	0.04

2.2. Experimental methodology

2.2.1. Mix design of UHPC

In this study, the modified Andreasen and Andersen model is utilized to design all the concrete mixtures, which reads as follows [43,86–88]:

$$P(D) = \frac{D^q - D_{min}^q}{D_{max}^q - D_{min}^q} \quad (1)$$

where D is the particle size (μm), $P(D)$ is a fraction of the total solids being smaller than size D, D_{max} is the maximum particle size (μm), D_{min} is the minimum particle size (μm) and q is the distribution modulus.

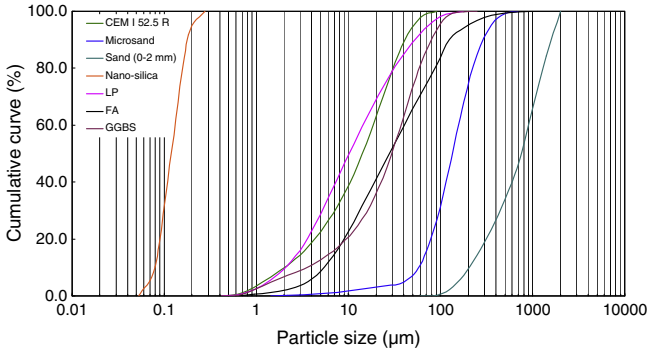

Fig. 1. Particle size distributions of the used materials.

As presented in the literature [44–47], different types of concrete can be designed using Eq. (1) by applying different values of the distribution modulus q, as it determines the proportion between the fine and coarse particles in the mixture. As recommended in [44], considering that a high amount of fine particles is utilized to produce the UHPC, the value of q is fixed at 0.23 in this study. The modified Andreasen and Andersen model (Eq. (1)) acts as a target function for the optimization of the composition of mixture of granular materials. The proportions of each individual material in the mix are adjusted until an optimum fit between the composed mix and the target curve is reached, using an optimization algorithm based on the Least Squares Method (LSM), as presented in Eq. (2). When the deviation between the target curve and the composed mix, expressed by the sum of the squares of the residuals (*RSS*) at defined particle sizes, is minimized, the composition of the concrete is considered the best one (optimized packing) [47].

$$RSS = \sum_{i=1}^{n} \left(P_{mix}(D_i^{i+1}) - P_{tar}(D_i^{i+1})\right)^2 \quad (2)$$

where P_{mix} is the composed mix, and the P_{tar} is the target grading calculated from Eq. (1).

The developed UHPC mixtures are listed in Table 5. In total, three different types of UHPC and one reference are designed, and three different water to binder ratios are chosen. Compared to the reference sample, about 30% of Portland cement (by mass) is replaced by FA, GGBS or LP in the UHPC mixtures. It can be noticed from Fig. 3, that the resulting integral grading curves of all the designed concretes are comparable to each other. The deviation between the target curves and composed mixes (RSS) are 101, 79, 85 and 74 for the reference mixture and the mixtures with FA, GGBS and LP, respectively.

2.2.2. Determination of water demand

In this study, the Puntke test is employed to evaluate the water demand of the powder materials (cement, FA, GGBS and LP). The water demand from Puntke test shows the water absorption capacity of the tested powder at the point of saturation, which depicts the transition from a coherent packing to a suspension [48]. Therefore, a fine, cohesion-free granular skeleton cannot be self-compacted to a specific packing density until the water content is sufficient for the saturation of the dense grain structure [44]. The first sign of bleeding is a glimmering surface of the water–powder mixture, which also is the evaluation target criterion of the addressed test. Additionally, Puntke test assumes that for the point of saturation the granular blend becomes free of air (the void fraction is completely filled with water), which derives a relation between the void fraction and the involved volumes of water and

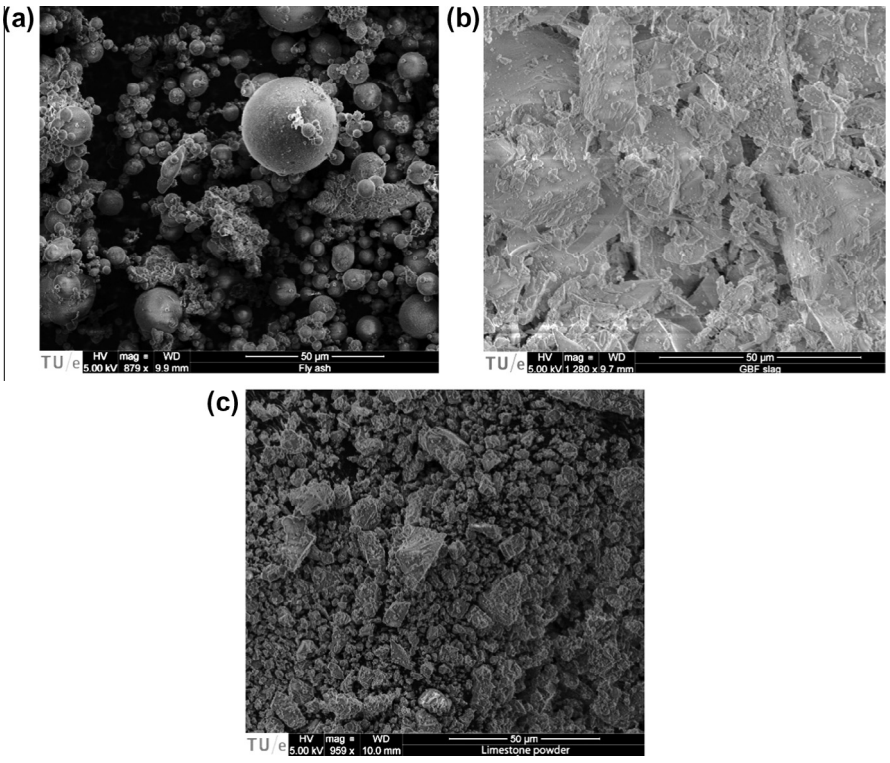

Fig. 2. SEM pictures of used FA (a), GGBS (b) and LP (c).

powder represented by their masses. Hence, void faction of the saturated powder material can be computed as follows [48]:

$$\psi = \frac{V_w}{V_p + V_w} \tag{3}$$

where ψ is the void faction of the saturated powder material, V_w is the volumetric water demand of the powder material for saturation, V_p is the volume of the tested powder material.

2.2.3. Mixing procedure

In this study, the mixing procedure follows the method shown in [40]:

(1) All powders and sand fractions are added into the mixer for dry mixing (30 s at low speed).
(2) Then, around 75% of water is added into the mixer. After mixing for 90 s (low speed), the mixer is stopped for 30 s.
(3) Afterwards, the remaining water and SP are added, and the mixture is mixed at low speed for 180 s.
(4) Finally, the mixture is mixed at high speed for 120 s.

The mixing is always executed under laboratory conditions with dried and tempered aggregates and powder materials. The room temperature while mixing and testing is constant at around 21 °C.

2.2.4. Flowability of UHPC

To evaluate the flowability of UHPC, the flow table tests are performed following EN 1015-3 [49]. During the test, the cone is lifted straight upwards in order to allow free flow of the mixture without any jolting (flowing suggestions from [44]). In the test, two diameters perpendicular to each other (d_1 (mm) and d_2 (mm)) are determined. Their mean is employed to compute the relative slump (Γ) via:

Table 5
Mix recipes of the designed concrete.

No.	C (kg/m^3)	FA (kg/m^3)	GGBS (kg/m^3)	LP (kg/m^3)	S (kg/m^3)	MS (kg/m^3)	nS (kg/m^3)	W (kg/m^3)	SP (kg/m^3)	W/B	SP/C
1	582.1	259.9	0	0	1039.5	216.6	24.3	173.2	43.3	0.2	0.07
2	591.9	264.3	0	0	1057.0	220.2	24.7	159.3	44.0	0.18	0.07
3	600.0	267.9	0	0	1071.4	223.2	25.0	147.8	44.6	0.165	0.07
4	596.1	0	266.1	0	1064.5	221.8	24.8	177.4	44.4	0.2	0.07
5	606.4	0	270.7	0	1082.9	225.6	25.3	163.2	45.1	0.18	0.07
6	614.9	0	274.5	0	1098.0	228.8	25.6	151.5	45.8	0.165	0.07
7	592.6	0	0	264.6	1058.3	220.5	24.7	176.4	44.1	0.2$^{\#}$	0.07
8	602.8	0	0	269.1	1076.5	224.3	25.1	162.2	44.9	0.18$^{\#}$	0.07
9	611.2	0	0	272.9	1091.4	227.4	25.5	150.6	45.5	0.165$^{\#}$	0.07
Ref. [1]	868.8	0	0	0	1072.5	223.4	25.0	178.8	44.7	0.2	0.05
Ref. [2]	883.9	0	0	0	1091.2	227.3	25.5	164.4	45.5	0.18	0.05
Ref. [3]	896.3	0	0	0	1106.6	230.5	25.8	152.7	46.1	0.165	0.05

C – Cement, FA – Fly ash, GGBS – Ground granulated blast-furnace slag – LP – Limestone powder, S – sand, MS – Microsand, nS – Nano-silica, W – Water, SP – Superplasticizer, W/B – water to binder ratio, SP/C – superplasticizer to cement ratio, Ref. – reference samples, and # – LP is considered as a binder in the calculation.

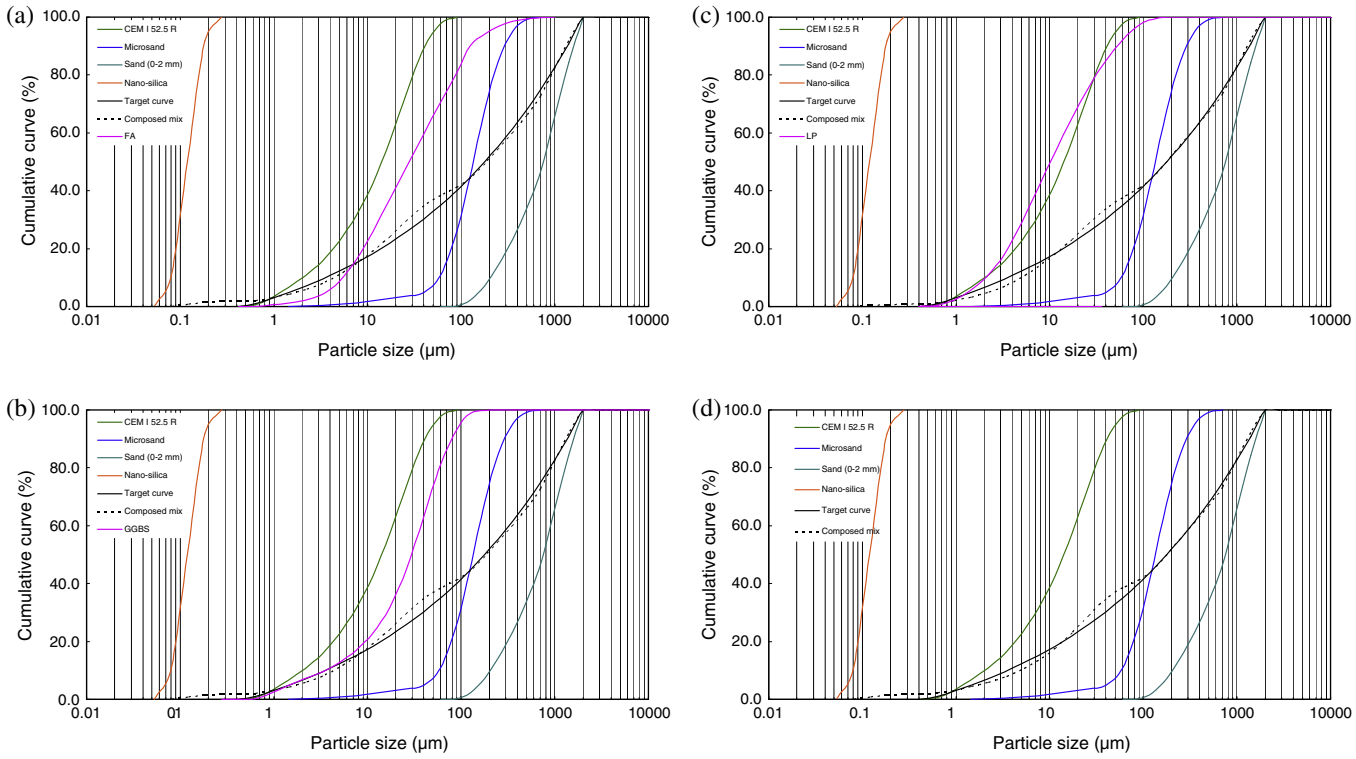

Fig. 3. PSDs of the ingredients, target and optimized grading curves of the designed concretes: (a) with FA, (b) with GGBS, (c) with LP and (d) reference mixture.

$$\Gamma = \left(\frac{d_1 + d_2}{2d_0}\right)^2 - 1 \tag{4}$$

where d_0 represents the base diameter of the used cone (mm), i.e. 100 mm in the case of the Hägermann cone. The relative slump Γ is a measure for the deformability of the mixture, which originally was introduced by Okamura and Ozawa [50] as the relative flow area R.

2.2.5. Mechanical properties of UHPC

After preforming the flowability tests, the fresh concrete is cast in molds with the dimensions of 40 mm × 40 mm × 160 mm. The prisms are demolded approximately 24 h after casting and then cured in water at about 21 °C. After curing for 28 and 91 days, the flexural and compressive strengths of the specimens are tested according to EN 196-1 [51]. At least three specimens are tested at each age to compute the average strength.

2.2.6. Water-permeable porosity of UHPC

The water-permeable porosity of the designed UHPC is measured applying the vacuum-saturation technique, which is referred to as the most efficient saturation method [52]. The saturation is carried out on at least 3 samples (100 mm × 100 mm × 20 mm) for each mix, following the description given in NT Build 492 [53] and ASTM C1202 [54].

The water permeable porosity is calculated from the following equation:

$$\varphi_{v,water} = \frac{m_s - m_d}{m_s - m_w} \cdot 100 \tag{5}$$

where $\varphi_{v,water}$ is the water permeable porosity (%), m_s is the mass of the saturated sample in surface-dry condition measured in air (g), m_w is the hydrostatic mass of water-saturated sample (g) and m_d is the mass of oven-dried sample (g).

2.2.7. Calorimetry analysis of UHPC

Following the recipes shown in Table 5, the pastes (without aggregates) are produced for the calorimetry analysis. The water to binder ratio of the prepared mixtures is fixed at 0.18 (based on the results of mechanical properties that will be shown later). All the pastes are mixed for two minutes and then injected into a sealed glass ampoule, which is then placed into the isothermal calorimeter (TAM Air, Thermometric). The instrument is set to a temperature of 20 °C. After 7 days, the measurement is stopped and the obtained data is analyzed. All results are ensured by double measurements (two-fold samples).

2.2.8. Thermal test and analysis of UHPC

A Netzsch simultaneous analyzer, model STA 449 C, is used to obtain the Thermo-gravimetric (TG) and Differential Scanning Calorimetry (DSC) curves of UHPC paste. The water to binder ratio of the tested sample is fixed at 0.18 (based on the results of mechanical properties that will be shown later). Analyses are conducted at the heating rate of 5 °C/min from 20 °C to 1000 °C in flowing nitrogen environment.

3. Experimental results and discussion

3.1. Fresh behavior of the designed UHPC

The relative slump of fresh UHPC mixtures versus the volumetric water to powder (particle size < 125 μm) ratio is presented in Fig. 4. As can be seen, with an increase of the water amount, the relative slump of all the concrete mixtures increases linearly. The intersection of these linear functions with the axis of ordinates at $\Gamma = 0$ depicts the retained water ratio where no slump takes place [50]. In other words, this denotes the maximum amount of water which can be retained by the particles. Exceeding this water content will turn the coherent bulk into a concentrated suspension [44]. In this study, it can be noticed that the water demand of each

mixture follow the order: FA (0.306) < LP (0.315) < GGBS (0.359) < reference sample (0.384). Nevertheless, these results are not in accordance with the results obtained from Puntke test (as shown in Table 3). This should be attributed to the following two reasons: (1) the used mineral admixtures are different from each other, which can also affect the workability of the concrete mixture. As presented in Fig. 2, a large amount of angular particles can be observed in GGBS, while that the FA particles are more spherical. The particle shape factors (shown in Table 3) of the used mineral admixtures are 1.20, 1.58 and 1.28 for FA, GGBS and LP, respectively [44]. When the shape factor is close to 1, the shape of the particle is spherical, which can further help to improve the flowability of the concrete mixture; (2) the utilized superplasticizer has different effect on the slump flow value of various powders. As described in [85], the efficiency of superplasticizer largely depends on the zeta potential along the entire surface of the tested powder particles. The experiments shown in [85] demonstrate that, in most cases, cement needs more superplasticizer to reach a certain slump flow value compared to that of FA, GGBS and LP. Hence, based on the two reasons mentioned above, the mixture with FA has the lowest demand water amount among all the analyzed concrete mixtures.

The slopes of the lines shown in Fig. 4, called the deformation coefficient, represent the sensitivity of the mixture to the water amount needed to attain a certain flowability [50]. When the value of deformation coefficient is relatively small, a big change in deformability can be observed (to a certain change in water dosage), which means the mixture tends to bleed or segregate sooner than the mixtures with larger deformation coefficients [44,55]. In this study, the obtained deformation coefficient values are small and similar to each other, which implies that all the designed mixtures are sensitive to the water amount. This should be attributed to the specific characteristics of UHPC, which has a large amount of superplasticizer and low water content. Hence, to achieve a well flowable UHPC mixture, the added water amount should be precisely controlled.

3.2. Mechanical properties of the designed UHPC

The flexural and compressive strengths of UHPC at 28 and 91 days are shown in Fig. 5. A very slight variation of the strengths can be observed when the water/binder ratio increases from 0.165 to 0.18. Nevertheless, with a further increase of the water/binder ratio (from 0.18 to 0.20), the mechanical properties of the produced UHPC decrease. This phenomenon is different from that shown in [27]. In most cases, due to the fact that the excessive water can enhance the porosity of concrete, the strengths of concrete gradually decrease with an increase of the water amount. The difference between the obtained results and the results presented in the literature should be attributed to the fact that a large amount of powder and limited water are utilized to produce the UHPC. When the water to binder ratio is relatively small, the added water is more significantly absorbed by the powders (cement, FA, GGBS or LP in this study), and cannot react with cement, which causes that the amount of cement hydration products is limited and the strength development of UHPC is restricted. Hence, in this study, the strengths difference between the mixtures with lowest and medium water amount is not significant. There is an optimal value of water/binder ratio, at which the strengths of the UHPC can be highest.

Furthermore, it can be found here the mixture with GGBS has superior mechanical properties at both 28 and 91 days, while that the strengths of the mixtures with FA or LP are similar to each other. The observed trend is conflicting with the results obtained for normal strength concrete [16–27]. Normally, the pozzolanic reaction of FA begins at the age of 3 days after blending with cement and water [56–58]. Nevertheless, this pozzolanic reaction is much slower than the Portland cement hydration [56–58]. The main hydrate of cement and fly-ash, calcium silicate hydrate (C–S–H), adopts two distinct morphologies: a low density C–S–H at the surface of cement and FA particles and a high density C–S–H deeper into the cement and FA particles [59,60]. After curing for 28 days, a limited amount of C–S–H gel can be generated, and the microstructure of the concrete is less dense than the one with GGBS. With an ongoing cement hydration, more portlandite can be generated and the pozzolanic reaction of FA can be accelerated, which causes that the already formed pore structure in concrete is filled by the newly generated C–S–H and the mechanical properties of concrete are significantly improved after curing for 91 days [22–27]. Nevertheless, in this study, the strengths of the mixture with FA are similar to that of the mixture with LP after curing for 91 days, which implies that the pozzolanic reaction of FA cannot proceed well in the cementitious system of UHPC (assuming limestone is a non-reactive material).

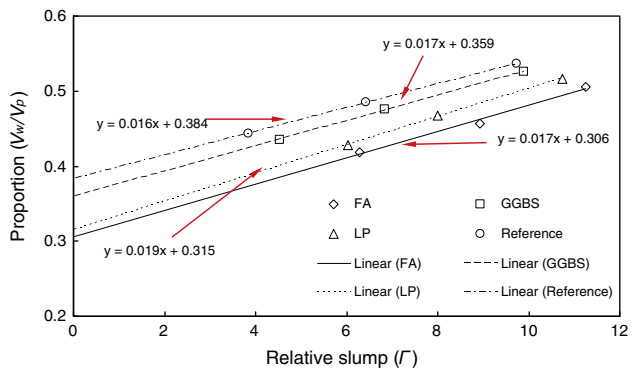

Fig. 4. Relative slump (Γ) versus volumetric water /powder ratio (V_w/V_p).

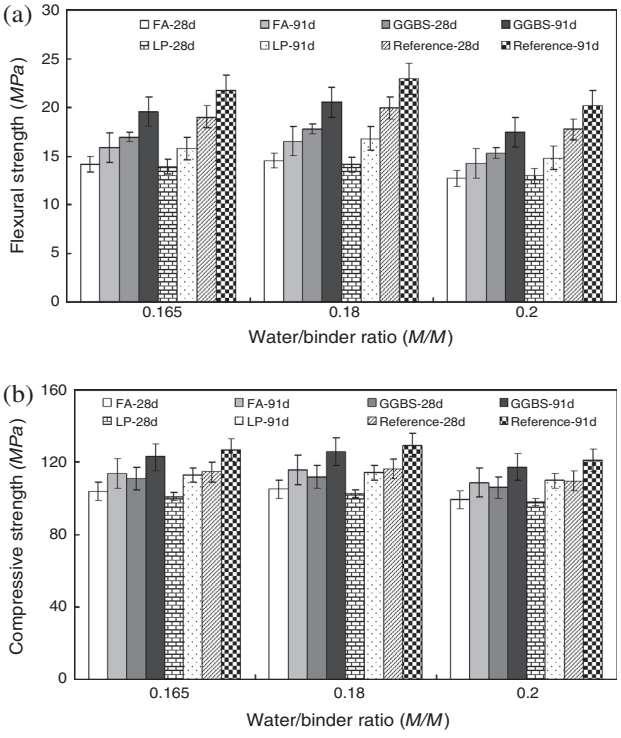

Fig. 5. Mechanical properties of the developed UHPC mixtures with different mineral admixtures and water amount: (a) flexural strength and (b) compressive strength.

From the results obtained in this study, it can be summarized that the specific system of UHPC (very low water amount and high SP content) can significantly influence the pozzolanic reaction of FA and mechanical properties of the hardened UHPC. As already mentioned, the strengths of the mixture with GGBS are superior, and comparable to the reference sample (with 50% more cement). To further investigate the pozzolanic reaction of FA/GGBS or their effect on cement hydration at early age, some other techniques (isothermal calorimetry, thermal analysis) are employed and presented later.

3.3. Water-permeable porosity of the designed UHPC

Fig. 6 illustrates the variation of the total water-permeable porosity (after curing for 28 or 91 days) of UHPC at different water to binder ratios. In accordance with the mechanical properties results, the water-permeable porosity of UHPC firstly remains stable and then increases with an increase of the water to binder ratio. This should also be attributed to the fact that a large amount of powder and limited water are utilized to produce the UHPC. When the water amount is relatively low, the added water is more significantly absorbed by the powders (cement, FA, GGBS or LP in this study), and cannot react with cement, which cause that the amount of cement hydration products is limited and the water-permeable porosity is relatively high. On the other hand, when the water content is higher, the excessive water can obviously enhance the porosity of concrete, as described in [27]. Hence, there is an optimal water to binder ratio, at which the water-permeable porosity of UHPC can be minimized. Moreover, it can also be found that the water-permeable porosity of the mixtures with FA or LP is relatively higher than that with GGBS and the reference mixture, which implies that the mechanical properties of the mixtures with FA and LP are lower than that of the mixture with GGBS.

To clearly determine the relationships between the water-permeable porosity and mechanical properties of UHPC, the results obtained here are compared with the existing models (as shown in Fig. 7). Historically, several general types of models have been developed for cement-based materials. From a study of the compressive strength of Al_2O_3 and ZrO_2, Ryshkewitch [61] proposed the following relationship:

$$\sigma = \sigma_0 \cdot \exp(-k \cdot p) \tag{6}$$

where σ is the strength, σ_0 is the strength at zero porosity, p is the porosity of the tested material and k is an empirical constant.

Balshin [62] suggested the following relationship:

$$\sigma = \sigma_0 \cdot (1-p)^b \tag{7}$$

where b is the empirical constant.

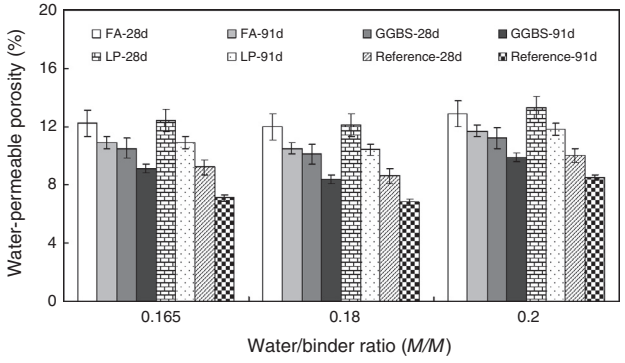

Fig. 6. Total water-permeable porosity of the designed UHPC with different mineral admixtures and water amount.

According to the investigation shown in [63], Chen et al. proposed the extended Zheng's model:

$$\sigma = \sigma_0 \cdot \left[\left(\frac{p_c - p}{p_c} \right)^{1.85} \cdot (1 - p^{2/3}) \right]^{1/2} \tag{8}$$

where p_c is the percolation porosity at failure threshold. In the present study, all the empirical constants for the models mentioned above are chosen as recommended in [63]. Based on the empirical fitting of the experimental data to the presented models, the maximum flexural and compressive strengths (σ_0) of the UHPC (when porosity is zero) are equal to 24 and 160 MPa, respectively.

From Fig. 7, it can be found that all the presented models can well represent the relationships between the water-permeable porosity and the compressive strength of the developed UHPC. However, these models are inaccurate in predicting the obtained relationships between the water-permeable porosity and the flexural strength. The existing models obviously underestimate the flexural strength of UHPC when its water-permeable porosity is less than about 8%. Additionally, these models also overestimate the flexural strength of UHPC when its water-permeable porosity is larger than 10%. These phenomena may be attributed to the relatively low water-permeable porosity and high strengths of UHPC. For normal concrete, the water-permeable porosity is relatively high, which is the reason for lower mechanical properties (especially the flexural strength). For instance, Safiuddin and Hearn [52] reported a porosity of 20.5% of concrete produced with a water/cement ratio of 0.60, employing the same porosity measurement method as used in the present study (vacuum-saturation technique). Many of these empirical formulas are derived for normal strength concrete (NSC). However, for UHPC, its porosity is very low and its flexural strength is around 3–4 times of that of NSC. Therefore, these empirical equations are less precise to

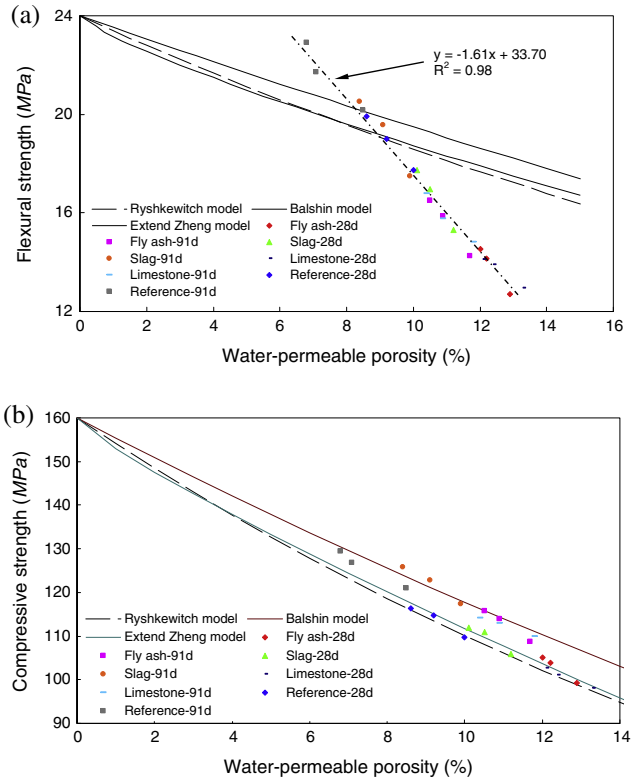

Fig. 7. Relationship between water-permeable porosity and flexural strength (a) and compressive strength (b) of the developed UHPC.

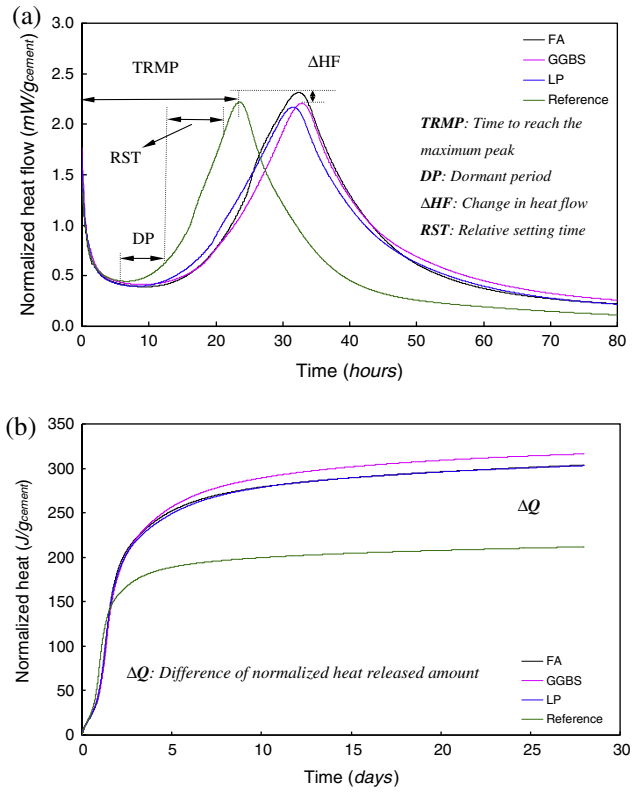

Fig. 8. Calorimetry test results of UHPC pastes with different mineral admixtures: (a) normalized heat flow and (b) normalized total heat.

represent the relationships between the water-permeable porosity and the flexural strength of the developed UHPC.

Based on the obtained results, a new relationship between the water-permeable porosity and the flexural strength of the UHPC is shown as follows:

$$\sigma = \left(\frac{p_c - p}{p_c}\right)\sigma_0 \tag{9}$$

in which the σ_0 is about 33.7 MPa, and the p_c is around 0.21. It can be noticed that the derived p_c value is much smaller than that recommended in [63] (0.78), which could be the reason that the existing models cannot well represent the relationships between the water-permeable porosity and the flexural strength of the developed UHPC. As mentioned before, compared to NSC, UHPC has much lower porosity and higher flexural strength. Therefore, to precisely establish the relationships between the water-permeable porosity and the flexural strength of UHPC, the crucial parameters should be reasonably adjusted.

3.4. Hydration kinetics of the designed UHPC

Based on the calorimetry test results, the influence of the different mineral admixtures on the cement hydration of UHPC is investigated and presented in Fig. 8. It is apparent that the influence of FA, GGBS or LP on the early hydration kinetics of the designed UHPC is very similar, which can be demonstrated by the relatively small difference between the observed dormant period (calculated as the time between the lower point of the heat flow curve and the first inflection point in the main peak), relative setting time (calculated as the time between the first and the second inflection points in the heat flow curve), as well as the time to reach the maximum hydration peak. This phenomenon is not in accordance with the results shown in [19,20,22,23,64]. In most cases, GGBS can quickly react with $Ca(OH)_2$ and generate the C–S–H gel, while the reaction between FA and portlandite is relatively slower. It is suggested that the fly ash surface acts as a Ca^{2+} sink, which is caused by the reaction of the aluminate in the fly ash with the Ca from the solution and/or chemisorption of Ca^{2+} ions on the fly ash surface [23,65]. This would retard the formation of C–S–H nuclei and thereby delay the end of the induction period. Hence, when the particle size distributions of GGBA, FA and LP are similar to each other, the activity of GGBS should be much higher than that of FA and LP in concrete at early age.

To better explain these phenomena, the following reasons should be considered: (1) a large amount of superplasticizer is utilized in the production of the UHPC. According to the investigation of Jansen [66], complex Ca^{2+} ions from pore solution by the superplasticizer can touch the polymer absorbed on the nuclei or the anhydrous grain surfaces, which in turn might lead to prevention of the nuclei growth or to the dissolution of the anhydrous grains. Hence, the early hydration of the cement is significantly retarded and the generation of $Ca(OH)_2$ is restrained. Due to the insufficient amount of portlandite in the mixtures, the pozzolanic reaction cannot well progress, which causes that the difference of the pozzolanic activity between FA and GGBS is not easy to be observed in the calorimetry tests; (2) low water content is used in the UHPC mixtures. To achieve good mechanical properties, high powder amount and low water content are normally used to produce UHPC, which causes that much water is absorbed by the powder materials and there is litter free water in the cementitious system. Hence, the diffusion of Ca^{2+} and OH^- is restricted, and pozzolanic reaction of FA or GGBS is simultaneously postponed.

The normalized (by 1 g of cement) total heat of the designed UHPC mixtures is illustrated in Fig. 8b. The total heat is the contribution of heat produced by the cement particles themselves and by the pozzolanic reaction between the active mineral admixtures and the precipitated $Ca(OH)_2$ [67]. The total heat can be related to the hydration degree of the paste, and this hydration degree is related to the compressive strength of the mixture, if the parameters of the microstructure are similar. Thus, a higher compressive strength is expected with the progressive increase of the total heat released. In this study, after 28 days it can be noticed that the normalized heat of the mixture with GGBS is the largest, which is followed by the one with FA and LP. As described before, due to effect of the large amount of superplasticizer and low water content in UHPC, the pozzolanic reaction of GGBS cannot well progress during the initial 5 days. However, afterwards, with an increasing concentration of $Ca(OH)_2$, the pozzolanic reaction of GGBS is promoted, which simultaneously causes that more heat can be released and the mechanical properties of the concrete can be enhanced. Additionally, the normalized heat of the mixture with FA is similar to that with LP, which implies that the FA and LP have similar contributions to the cement hydration after 28 days. Additionally, it can be found that the normalized heat of reference sample is significantly lower than the mixtures with mineral admixtures. This should be attributed to the fact that the calculation of normalized heat is based on the released heat per gram cement, and in the mixtures with mineral admixtures the utilized cement amount is obviously lower than that of reference sample.

Consequently, according to the results obtained in this study, it can be found that the hydration kinetics of UHPC is different from that of normal concrete. Due to the effects related to the superplasticizer and water dosages, the cement hydration and pozzolanic reaction of mineral admixtures are significantly retarded.

3.5. Thermal analysis of the hardened UHPC

The DSC and TG curves of the UHPC pastes after hydrating for 28 and 91 days are presented in Figs. 9 and 10. From the DSC

curves, it is apparent that there main peaks exist in the vicinity of 105 °C, 450 °C and 800 °C for all the samples, which can be attributed to the evaporation of free water, decomposition of $Ca(OH)_2$ and decomposition of $CaCO_3$, respectively [68–72]. Based on the test results shown in Figs. 9a and 10a, the samples for TG analysis were subjected to isothermal treatment during the test, which was set at 105 °C, 450 °C and 800 °C for 2 h. From the obtained TG curves, it can be noticed that all the tested samples show a similar tendency of losing their weight. However, their weight loss rates in each temperature range are different, which means that the amounts of the substances reacting at each treatment stage are different. It is important to note that the mass loss of portlandite of the mixture with GGBS is the smallest at 28 days, which implies that the pozzolanic activity of GGBS is relatively higher so that more portlandite has already been consumed. Fig. 8 confirms this phenomenon. However, after curing for 91 days, the mass loss of portlandite still follows the order: GGBS < FA < LP < reference concrete, while the differences between the mixtures with FA and LP is relatively small. Hence, it can be concluded that the specific cementitious system of UHPC significantly restricts the pozzolanic reaction of FA, which causes that a very limited amount FA can react with $Ca(OH)_2$ even after 91 days. Hence, it explains why the mechanical properties of the mixture with FA are lower than that with GGBS at both 28 and 91 days. The observed phenomenon is not in accordance with the results obtained in normal concrete system. As mentioned before, with the increase of the portlandite amount, the pozzolanic reaction of FA can be promoted, and the already-formed pore structure in concrete is filled by the newly generated C–S–H [16–21]. Consequently, it is not reliable to predict the effect of FA on the properties of UHPC, based on the results obtained on traditional concrete. Additionally, it can be noticed that the difference of the $Ca(OH)_2$ amount between the mixtures with mineral admixtures is relatively small. This phenomenon may be attributed to the reaction between nano-silica and $Ca(OH)_2$, which cause that very limited $Ca(OH)_2$ is available to react with FA or GGBS.

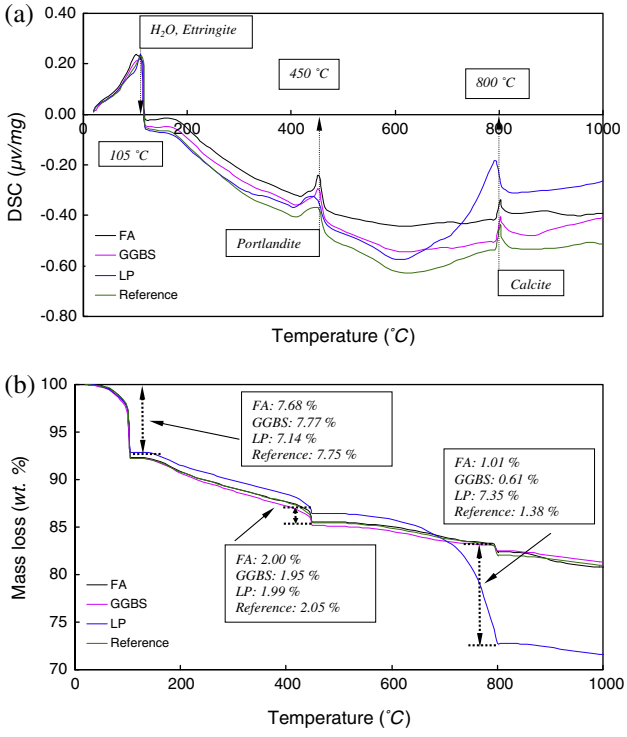

Fig. 9. Thermal analysis results of UHPC pastes with different mineral admixtures (after hydrating for 28 days): (a) DSC curves and (b) TG curves.

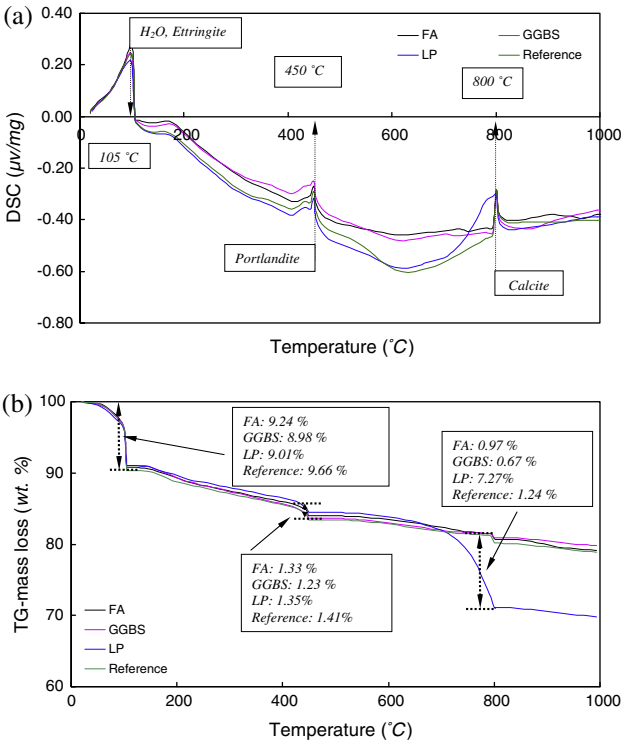

Fig. 10. Thermal analysis results of UHPC pastes with different mineral admixtures (after hydrating for 91 days): (a) DSC curves and (b) TG curves.

According to the thermal analyses results, it is clear that there is more portlandite in the concrete with larger amount of cement (e.g. the reference system in this study) than the mixture with mineral admixtures, which does not play a positive role in improving the mechanical properties of concrete, especially when the portlandite hexagonal plates form distribute around the ITZ. When cement is appropriately replaced by GGBS, portlandite amount can be reduced and the already-formed pore structure in concrete can be filled by the newly generated C–S–H. Consequently, the UHPC with good mechanical properties can be produced with relatively low cement amount.

3.6. Ecological evaluation of the designed UHPC

To demonstrate that the designed UHPC is materials efficient and eco-friendly, its embedded CO_2 emission is evaluated in this study, focusing on the amount of materials required for 1 m^3 of compacted concrete. Based on the embodied CO_2 values for each components of concrete [74,89], the relationships between the CO_2 emission and the compressive strength of UHPCs are illustrated in Fig. 11. It can be noticed that the enhancement of compressive strength of all the analyzed UHPCs corresponds to an increase of the embedded CO_2 emission and environmental impact. Some of the presented UHPCs have superior mechanical properties (compressive strength is more than 200 MPa), but simultaneously, their embedded CO_2 emissions are also high (more than 1200 kg/m^3 concrete). However, it is important to notice that the data points representing UHPC developed in this study are all below of the trend line, which means the designed UHPC has a lower environmental impact than the other UHPCs. This is significant especially for the mixture with GGBS, as its compressive strength is larger than that with FA and LP, with a comparable embedded CO_2 emission at the same age. Additionally, it can be also found that the data points representing the reference concrete developed

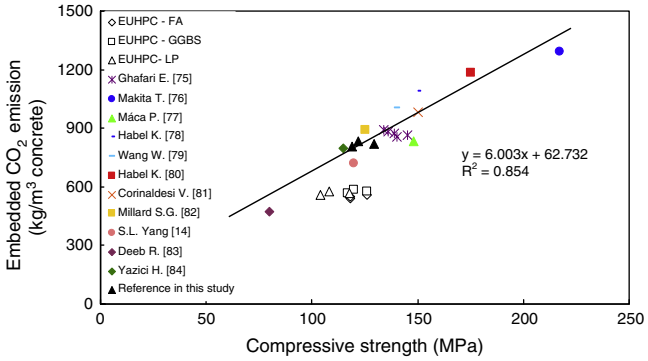

Fig. 11. Comparison of embedded CO_2 emission of the developed eco-friendly UHPC (EUHPC) and other UHPCs or UHPFRCs [14,75–84].

in this study are on the trend line, which implies that the relatively high cement amount is not helpful for producing UHPC with small environmental impact. This should be attributed to the fact that when the cement amount is relatively high, the cement hydration degree is smaller and the cement efficiency is lower, compared to the concrete with low cement amount [40]. Hence, to efficiently produce an eco-friendly UHPC with a reduced environmental impact, the mineral admixtures should be utilized to replace cement and the concrete design should be based on the optimized particle packing model.

4. Conclusions

This paper presents the mix design and properties evaluation of an eco-friendly Ultra-High Performance Concrete (UHPC). From the results presented in this paper the following conclusions are drawn:

- In this study, based on the modified Andreasen & Andersen particle packing model, UHPC with different mineral admixtures (FA, GGBA, and LP) is produced. After comparing the embedded CO_2 emissions of the designed UHPC and other UHPCs, it is demonstrated that the proposed methodology allows production of an eco-friendly concrete with a relatively low environmental impact.
- The fresh behavior of the developed UHPC is evaluated. It is found that the water demand of each UHPC mixtures with FA, GGBS, LP and reference concrete follows the order: FA < LP < GGBS < reference. Moreover, the deformation coefficient values of UHPCs are small and close to each other, which implies that all the designed mixtures are sensitive to the water amount.
- The mechanical properties of UHPC with GGBS are obviously higher than that with FA or LP at both 28 and 91 days. Furthermore, a slight increase of the strengths can be observed when the water/binder ratio increases from 0.165 to 0.18. Nevertheless, with a further increase of the water/binder ratio (from 0.18 to 0.20), the mechanical properties of the produced UHPC decrease.
- The existing models used to correlate the porosity and mechanical properties of concrete obviously underestimate the flexural strength of UHPC when its water-permeable porosity is less than about 8%, and overestimate the flexural strength of UHPC when its water-permeable porosity is larger than 10%. At the same time, all the presented models can well represent the relationships between the water-permeable porosity and the compressive strength of the designed UHPC.
- The hydration heat development curves of the UHPC mixtures with FA, GGBS and LP are similar to each other during the initial five days. Afterwards, the hydration rate of the mixture with GGBS is obviously accelerated. Due to the specific cementitious system of UHPC (very small water/binder ratio and relatively high SP amount), it is observed that the pozzolanic reaction of FA is significantly retarded, which causes that a very limited amount of FA can react with $Ca(OH)_2$ after curing for 91 days.

Acknowledgements

The authors wish to express their gratitude to Ir. G.C.H. Doudart de la Grée for assisting with the XRF and SEM testing, experimental work and valuable discussions. Moreover, the appreciation also goes to the following sponsors of the Building Materials research group at TU Eindhoven: Graniet-Import Benelux, Kijlstra Betonmortel, Struyk Verwo, Attero, ENCI, Provincie Overijssel, Rijkswaterstaat Zee en Delta – District Noord, Van Gansewinkel Minerals, BTE, V.d. Bosch Beton, Selor, Twee "R" Recycling, GMB, Schenk Concrete Consultancy, Geochem Research, Icopal, BN International, Eltomation, Knauf Gips, Hess ACC Systems, Kronos, Joma, CRH Europe Sustainable Concrete Centre, Cement&BetonCentrum and Heros (in chronological order of joining).

References

[1] Olivier B, Christian V, Micheline M, Pierre-Claude A. Characterization of the granular packing and percolation threshold of reactive powder concrete. Cem Concr Res 2000;30:1861–7.
[2] Richard P, Cheyrezy M. Composition of reactive powder concretes. Cem Concr Res 1995;25(7):1501–11.
[3] Chan Y, Chu S. Effect of silica fume on steel fiber bond characteristics in reactive powder concrete. Cem Concr Res 2004;34(7):1167–72.
[4] Zhang Y, Sun W, Liu S, Jiao C, Lai J. Preparation of C200 green reactive powder concrete and its static–dynamic behaviors. Cem Concr Comp 2008;30(9):831–8.
[5] Yazici H, Deniz E, Baradan B. The effect of autoclave pressure, temperature and duration time on mechanical properties of reactive powder concrete. Constr Build Mater 2013;42:53–63.
[6] Rossi P. Influence of fibre geometry and matrix maturity on the mechanical performance of ultra-high-performance cement-based composites. Cem Concr Comp 2013;37:246–8.
[7] El-Dieb AS. Mechanical, durability and microstructural characteristics of ultra-high-strength self-compacting concrete incorporating steel fibres. Mater Des 2009;30:4286–92.
[8] Hassan AMT, Jones SW, Mahmud GH. Experimental test methods to determine the uniaxial tensile and compressive behaviour of ultra-high performance fibre reinforced concrete (UHPFRC). Constr Build Mater 2012;37:874–82.
[9] UNSTATS. Greenhouse gas emissions by sector (absolute values). United Nation Statistical Division: Springer; 2010.
[10] Friedlingstein P, Houghton RA, Marland G, Hackler J, Boden TA, Conway TJ, et al. Uptake on CO $_2$ emissions. Nat Geosci 2010;3:811–2.
[11] Habert G, Denarié E, Šajna A, Rossi P. Lowering the global warming impact of bridge rehabilitations by using Ultra High Performance Fibre Reinforced Concretes. Cem Concr Comp 2013;38:1–11.
[12] Tuan NV, Ye G, Breugel K, Copuroglu O. Hydration and microstructure of ultra-high performance concrete incorporating rice husk ash. Cem Concr Res 2011;41:1104–11.
[13] Tuan NV, Ye G, Breugel K, Fraaij ALA, Dai BD. The study of using rice husk ash to produce ultra-high performance concrete. Constr Build Mater 2011;25:2030–5.
[14] Yang SL, Millard SG, Soutsos MN, Barnett SJ, Le TT. Influence of aggregate and curing regime on the mechanical properties of ultra-high performance fibre reinforced concrete (UHPFRC). Constr Build Mater 2009;23:2291–8.
[15] Tayeh BA, Abu Bakar BH, Megat Johari MA, Voo YL. Mechanical and permeability properties of the interface between normal concrete substrate and ultra-high performance fibre concrete overlay. Constr Build Mater 2012;36:538–48.
[16] Regourd M, Thomassin JH, Baillif P, Touray JC. Blast-furnace GGBS hydration surface analysis. Cem Concr Res 1983;13:549–56.
[17] Regourd M. Structure and behavior of GGBS cement hydrates. Principal Paper III, 2, VII th Int congress chemistry of cement, Paris. 1980; I(III.2): 9–26.
[18] Thomassin JH, Goni J, Baillif P, Touray JC, Jaurand NC. An XPS study of the dissolution kinetics of chrysotile in 0.1n oxalic acid at different temperatures. Phys Chem Miner 1977;1:385–98.

[19] Wu X, Roy DM, Langton CA. Early stage hydration of GGBS-cement. Cem Concr Res 1983;13(2):277–86.
[20] Hwang CL, Shen DH. The effects of blast-furnace GGBS and FA on the hydration of portland cement. Cem Concr Res 1991;21(4):410–25.
[21] Wu X, Jiang W, Roy DM. Early activation and properties of GGBS cement. Cem Concr Res 1990;20(6):961–74.
[22] He J, Barry ES, Della MR. Hydration of FA-portland cements. Cem Concr Res 1984;14(4):505–12.
[23] Wei F, Michael WG, Della MR. The retarding effects of FA upon the hydration of cement pastes: the first 24 hours. Cem Concr Res 1985;15(1):174–84.
[24] Kovács R. Effect of the hydration products on the properties of fly-ash cements. Cem Concr Res 1975;5(1):73–82.
[25] Berry EE, Hemmings RT, Cornelius BJ. Mechanisms of hydration reactions in high volume FA pastes and mortars. Cem Concr Comp 1990;12(4):253–61.
[26] Feldman RF, Carette GG, Malhotra VM. Studies on mechanics of development of physical and mechanical properties of high-volume FA-cement pastes. Cem Concr Comp 1990;12(4):245–51.
[27] Neville AM. Properties of concrete. Burnt Mill, Harlow, England: Longman House; 1995.
[28] Soroka I, Setter N. The effect of fillers on strength of cement mortars. Cem Concr Res 1977;7(4):449–56.
[29] Kevin DI, Kenneth ED. A review of LP additions to Portland cement and concrete. Cem Concr Comp 1991;13(3):165–70.
[30] Valcuende M, Parra C, Marco E, Garrido A, Martínez E, Cánoves J. Influence of LP filler and viscosity-modifying admixture on the porous structure of self-compacting concrete. Constr Build Mater 2012;28(1):122–8.
[31] Bentz DP. Modeling the influence of LP filler on cement hydration using CEMHYD3D. Cem Concr Comp 2006;28(2):124–9.
[32] Bessey GE. Proceedings of the symposium on the chemistry of cements, Stockholm, Ingeniarsveterskapsakaderrier, Stockholm; 1938. p. 233–4.
[33] Lea FM. The chemistry of cement and concrete. New York: Chemical publishing company; 1971. p. 202–33.
[34] Carlson ET, Berman HA. Some observations on the calcium aluminate carbonate hydrates. J Res Nat Bur Stand 1960;64A(4):333–41.
[35] Kumar A, Oey T, Kim S, Thomas D, Badran S, Li J, et al. Simple methods to estimate the influence of LP fillers on reaction and property evolution in cementitious materials. Cem Concr Comp 2013;42:20–9.
[36] De Larrard F, Sedran T. Optimization of ultra-high-performance concrete by the use of a packing model. Cem Concr Res 1994;24:997–1009.
[37] De Larrard F, Sedran T. Mixture-proportioning of high-performance concrete. Cem Concr Res 2002;32:1699–704.
[38] Fennis SAAM, Walraven JC, den Uijl JA. The use of particle packing models to design ecological concrete. Heron 2009;54:185–204.
[39] Andreasen AHM, Andersen J. Über die Beziehungen zwischen Kornabstufungen und Zwischenraum in Produkten aus losen Körnern (mit einigen Experimenten). Kolloid-Zeitschrift 1930;50:217–28 [in German].
[40] Yu R, Spiesz P, Brouwers HJH. Mix design and properties assessment of Ultra-High Performance Fibre Reinforced Concrete (UHPFRC). Cem Concr Res 2014;56:29–39.
[41] Yu R, Spiesz P, Brouwers HJH. Effect of nano-silica on the hydration and microstructure development of Ultra-High Performance Concrete (UHPC) with a low binder amount. Constr Build Mater 2014;65:140–50.
[42] Yu R, Tang P, Spiesz P, Brouwers HJH. A study of multiple effects of nano-silica and hybrid fibres on the properties of Ultra-High Performance Fibre Reinforced Concrete (UHPFRC) incorporating waste bottom ash (WBA). Constr Build Mater 2014;60:98–110.
[43] Funk JE, Dinger DR. Predictive process control of crowded particulate suspensions, applied to ceramic manufacturing. Boston, United States: Kluwer Academic Publishers; 1994.
[44] Hunger M. An integral design concept for ecological self-compacting concrete. PhD thesis. Eindhoven University of Technology, Eindhoven, the Netherlands; 2010.
[45] Yu QL, Spiesz P, Brouwers HJH. Development of cement-based lightweight composites – Part 1: mix design methodology and hardened properties. Cem Concr Comp 2013;44:17–29.
[46] Spiesz P, Yu QL, Brouwers HJH. Development of cement-based lightweight composites – Part 2: durability related properties. Cem Concr Comp 2013;44:30–40.
[47] Hüsken G. A multifunctional design approach for sustainable concrete with application to concrete mass products. PhD thesis. Eindhoven University of Technology, Eindhoven, the Netherlands; 2010.
[48] Puntke W. Wasseranspruch von feinen Kornhaufwerken. Beton 2002;52(5):242–8 [in German].
[49] BS-EN-1015-3. Methods of test for mortar for masonry - Part 3: Determination of consistence of fresh mortar (by flow table). British Standards Institution-BSI and CEN European Committee for Standardization; 2007.
[50] Okamura H, Ozawa K. Mix-design for self-compacting concrete. Concr Library JSCE 1995;25:107–20.
[51] BS-EN-196-1. Methods of testing cement - Part 1: Determination of strength. British Standards Institution-BSI and CEN European Committee for Standardization; 2005.
[52] Safiuddin Md, Hearn N. Comparison of ASTM saturation techniques for measuring the permeable porosity of concrete. Cem Concr Res 2005;35:1008–13.
[53] NT Build 492. Concrete, mortar and cement-based repair materials: Chloride migration coefficient from non-steady-state migration experiments. Nordtest method, Finland; 1999.
[54] ASTM C1202. Standard test method for electrical indication of concrete's ability to resist chloride ion penetration. In: Annual book of ASTM standards, vol. 04.02. American Society for Testing and Materials, Philadelphia, July 2005.
[55] Quercia BG, Hüsken G, Brouwers HJH. Water demand of amorphous nano silica and its impact on the workability of cement paste. Cem Concr Res 2012;42:344–57.
[56] Zeng Q, Li K, Fen-chong T, Dangla P. Determination of cement hydration and pozzolanic reaction extents for fly-ash cement pastes. Constr Build Mater 2012;27:560–9.
[57] Papadakis VG. Effect of FA on Portland cement systems Part I: low-calcium FA. Cem Concr Res 1999;29:1727–36.
[58] Hanehara S, Tomosawa F, Kobayakawaa M, Hwang K. Effects of water/powder ratio, mixing ratio of FA, and curing temperature on pozzolanic reaction of FA in cement paste. Cem Concr Res 2001;31:31–9.
[59] Li C, Sun H, Li L. A review: the comparison between alkali-activated GGBS (Si + Ca) and metakaolin (Si + Al) cements. Cem Concr Res 2010;40:1341–9.
[60] Constantinides G, Ulm FJ. The nanogranular nature of C–S–H. J Mech Phys Solids 2007;55:64–90.
[61] Ryshkevitch R. Compression strength of porous sintered alumina and zirconia. J Am Ceram Soc 1953;36(2):65–8.
[62] Balshin MY. Relation of mechanical properties of powder metals and their porosity and the ultimate properties of porous-metal ceramic materials. Dokl Askd SSSR 1949;67(5):831–4.
[63] Chen X, Wu S, Zhou J. Influence of porosity on compressive and tensile strength of cement mortar. Constr Build Mater 2013;40:869–74.
[64] Schutter GD. Hydration and temperature development of concrete made with blast-furnace GGBS cement. Cem Concr Res 1999;29:143–9.
[65] Ogawa K, Uchikawa H, Takemoto K, Yasui I. The mechanism of the hydration in the system C_3S-pozzolana. Cem Concr Res 1980;10:683–96.
[66] Jansen D, Neubauer J, Goetz-Neunhoeffer F, Haerzschel R, Hergeth WD. Change in reaction kinetics of a Portland cement caused by a superplasticizer – calculation of heat flow curves from XRD data. Cem Concr Res 2012;42(2):327–32.
[67] Hewlett PC. Lea's chemistry of cement and concrete. 3th ed. New York: John Wiley & Son Inc.; 1988. pp. 1–1053.
[68] Alonso C, Fernandez L. Dehydration and rehydration processes of cement paste exposed to high temperature environments. J Mater Sci 2004;39(9):3015–24.
[69] Alarcon-Ruiz L, Platret G, Massieu E, Ehrlacher A. The use of thermal analysis in assessing the effect of temperature on a cement paste. Cem Concr Res 2005;35(3):609–13.
[70] Castellote M, Alonso C, Andrade C, Turrillas X, Campo J. Composition and microstructural changes of cement pastes upon heating, as studied by neutron diffraction. Cem Concr Res 2004;34(9):1633–44.
[71] Grattan-Bellew PE. Microstructural investigation of deteriorated Portland cement concretes. Constr Build Mater 1996;10(1):3–16.
[72] Handoo SK, Agarwal S, Agarwal SK. Physicochemical, mineralogical, and morphological characteristics of concrete exposed to elevated temperatures. Cem Concr Res 2002;32(7):1009–18.
[73] Yu R, Spiesz P, Brouwers HJH. Static properties and impact resistance of a green Ultra-High Performance Hybrid Fibre Reinforced Concrete (UHPHFRC): experiments and modeling. Constr Build Mater 2014;68:158–71.
[74] King D. The effect of silica fume on the properties of concrete as defined in concrete society report 74, cementitious materials. In: 37th Conference on our world in concrete and structures, Singapore, 29–31 August 2012.
[75] Ghafari E, Costa H, Júlio E, Portugal A, Durães L. The effect of nanosilica addition on flowability, strength and transport properties of ultra high performance concrete. Mater Des 2014;59:1–9.
[76] Makita T, Brühwiler E. Tensile fatigue behaviour of Ultra-High Performance Fibre Reinforced Concrete combined with steel rebars (R-UHPFRC). Int J Fatigue 2014;59:145–52.
[77] Máca P, Sovják R, Konvalinka P. Mix design of UHPFRC and its response to projectile impact. Int J Impact Eng 2014;63:158–63.
[78] Habel K, Gauvreau P. Response of ultra-high performance fiber reinforced concrete (UHPFRC) to impact and static loading. Cem Concr Comp 2008;30(10):938–46.
[79] Wang W, Liu J, Agostini F, Davy CA, Skoczylas F, Corvez D. Durability of an Ultra High Performance Fiber Reinforced Concrete (UHPFRC) under progressive aging. Cem Concr Res 2014;55:1–13.
[80] Habel K, Viviani M, Denarié E, Brühwiler E. Development of the mechanical properties of an Ultra-High Performance Fiber Reinforced Concrete (UHPFRC). Cem Concr Res 2006;36(7):1362–70.
[81] Corinaldesi V, Moriconi G. Mechanical and thermal evaluation of Ultra High Performance Fiber Reinforced Concretes for engineering applications. Constr Build Mater 2012;26(1):289–94.
[82] Millard SG, Molyneaux TCK, Barnett SJ, Gao X. Dynamic enhancement of blast-resistant ultra high performance fibre-reinforced concrete under flexural and shear loading. Int J Impact Eng 2010;37(4):405–13.
[83] Deeb R, Ghanbari A, Karihaloo BL. Development of self-compacting high and ultra high performance concretes with and without steel fibres. Cem Concr Comp 2012;34(2):185–90.
[84] Yazici H. The effect of curing conditions on compressive strength of ultra high strength concrete with high volume mineral admixtures. Build Environ 2007;42(5):2083–9.

[85] Schmidt W. Design concepts for the robustness improvement of self-compacting concrete. PhD thesis. Eindhoven University of Technology, Eindhoven, the Netherlands; 2014.
[86] Plum NM. The predetermination of water requirement and optimum grading of concrete. Copenhagen: The Danish National Institute of Building Research; 1950.
[87] Brouwers HJH, Radix HJ. Self compacting concrete: theoretical and experimental study. Cem Concr Res 2005;35:2116–36.
[88] Hüsken G, Brouwers HJH. A new mix design concept for each-moist concrete: a theoretical and experimental study. Cem Concr Res 2008;38:1249–59.
[89] Randl N, Steiner T, Ofner S, Baumgartner E, Mészöly T. Development of UHPC mixtures from an ecological point of view. Constr Build Mater 2014;67:373–8.